Soft Matter

PAPER

View Article Online
View Journal | View Issue

Cite this: *Soft Matter*, 2014, **10**, 5618

Surface effects on the structure and mobility of the ionic liquid C_6C_1ImTFSI in silica gels†

Moheb Nayeri,*[a] Matthew T. Aronson,[b] Diana Bernin,[c] Bradley F. Chmelka[b] and Anna Martinelli*[a]

Received 24th March 2014
Accepted 9th June 2014

DOI: 10.1039/c4sm00642a

www.rsc.org/softmatter

We report on how the dynamical and structural properties of the ionic liquid 1-hexyl-3-methylimidazolium bis(trifluoromethanesulfonyl)imide (C_6C_1ImTFSI) change upon different degrees of confinement in silica gels. The apparent diffusion coefficients of the individual ions are measured by ^{1}H and ^{19}F pulsed field gradient nuclear magnetic resonance (PFG-NMR) spectroscopy, while the intermolecular interactions in the ionogels are elucidated by Raman spectroscopy. In addition, the local structure of the ionic liquid at the silica interface is probed by solid-state NMR spectroscopy. Importantly, we extend this study to a wider range of ionic liquid-to-silica molar ratios (x) than has been investigated previously, from very low (high degree of confinement) to very high (liquid-like gels) ionic liquid contents. Diffusion NMR measurements indicate that a solvation shell, with a significantly lower mobility than the bulk ionic liquid, forms at the silica interface. Additionally, the diffusion of the $C_6C_1Im^+$ and $TFSI^-$ ions decreases more rapidly below an observed molar ratio threshold ($x < 1$), with the intrinsic difference in the self-diffusion coefficient between the cation and anion becoming less pronounced. For ionic liquid molar ratio of $x < 1$, Raman spectroscopy reveals a different conformational equilibrium for the $TFSI^-$ anions compared to the bulk ionic liquid, with an increased population of the *cisoid* isomers with respect to the *transoid*. Concomitantly, at these high degrees of confinement the $TFSI^-$ anion experiences stronger ion–ion interactions as indicated by the evolution of the $TFSI^-$ characteristic vibrational mode at ~740 cm^{-1}. Furthermore, solid-state 2D ^{29}Si{^{1}H} HETCOR NMR measurements establish the interactions of the ionic liquid species with the silica surface, where the presence of adsorbed water results in weaker interactions between ^{29}Si surface moieties and the hydrophobic alkyl protons of the cationic $C_6C_1Im^+$ molecules.

1 Introduction

Ionogels‡ are conceptually new materials obtained by the confinement of ionic liquids in a silica network.[1,2] Such networks can be achieved through the gelation of colloidal silica particles in the ionic liquid,[3–6] or *via* sol–gel synthesis protocols. In the latter case, the ionic liquid can be incorporated by swelling previously prepared gels§ or by directly using the ionic liquid as a solvent in the sol–gel reaction. The direct sol–gel approach is more straightforward and results in a more intimate biphasic system.[8,9]

The use of ionic liquids as solvents in the sol–gel synthesis of silica aerogels was proposed by Dai *et al.* in 2000.[10] The silica aerogels obtained by this method are mesoporous structures characterized by high surface area with potential applications in fields such as chemical separations and heterogeneous catalysis.[11–13] More recently, the same sol–gel process has been proposed as a means of confining ionic liquids within a solid matrix.[14] The resulting solid-like materials are interesting candidates for solid electrolytes in next-generation electrochemical devices[15,16] such as solar cells,[17] batteries,[18,19] and fuel cells.[9,20,21]

The degree to which the ion–wall interactions in the ionogel influence the physicochemical properties of the ionic liquid is an important issue to investigate, from the standpoints of fundamental understanding and technological application. Additionally, the confinement of the ionic liquid may also affect its properties compared to those in the bulk state. It is now well known that many ionic liquids separate into nano-scaled polar and non-polar domains,[22–24] where a liquid–solid (or liquid–gas)

[a]*Applied Surface Chemistry, Chemical and Biological Engineering, Chalmers University of Technology, Gothenburg, Sweden. E-mail: moheb.nayeri@chalmers.se; anna.martinelli@chalmers.se*

[b]*Department of Chemical Engineering, University of California, Santa Barbara, California 93106, USA*

[c]*Swedish NMR Centre, University of Gothenburg, Gothenburg, Sweden*

† Electronic supplementary information (ESI) available. See DOI: 10.1039/c4sm00642a

‡ The term ionogel has been used in other contexts to describe materials such as self-assembled glycopider in ionic liquids. In this article, however, ionogel refers specifically to ionic liquid-containing silica gels.

§ In this case, silica aerogels are prepared *via* the traditional sol–gel process using silica precursors in water–alcohol solutions.[7]

interface will lead to an inevitable break in this structuring. It is therefore important to understand how the ions reorder at an interface and how far this reordering propagates, as these processes will affect the properties of the ionogel as a whole.

With respect to future use of ionogels as electrolytes, a crucial property to investigate is the ionic mobility. Complex impedance spectroscopy of a silica ionogel containing *ca.* 80 vol% ionic liquid showed a reduction in ionic conductivity of approximately 50%.[14] Similarly, a recent study using ^{1}H pulsed field gradient nuclear magnetic resonance (PFG-NMR) showed that the apparent self-diffusion coefficient for the ionic liquid 1-butyl-3-methylimidazolium bis(trifluoromethanesulfonyl)imide (C_4C_1ImTFSI) decreased 3 to 10 fold depending on the filling factor with respect to the available volume in the mesoporous silica.[25] An interesting aspect in the context of mobility and conductivity is that by functionalizing the silica surface or mixing a third compound with the ionic liquid, the ionic conductivity of the ionogel can be increased by several orders of magnitude.[26]

Along with ionic mobility, other properties can be affected by confinement and ion–wall interactions. For example, ionogels prepared by *in situ* confinement of the ionic liquid through the sol–gel synthesis have shown much lower specific heat capacities than both the bulk ionic liquid and ionogels obtained by swelling previously prepared silica aerogels.[27] Confinement can also strongly affect the phase behavior of some ionic liquids. In silica networks, the melting temperature of the ionic liquid can significantly decrease depending on the degree of confinement and the anion's molecular structure.[7,8¶] In contrast, confinement of the ionic liquid 1-butyl-3-methylimidazolium hexafluorophosphate (C_4C_1ImPF$_6$) within carbon nanotubes has shown to increase the freezing temperature by several hundreds of degrees.[28] Additionally, atomic force microscopy (AFM) measurements have shown that thin layers of the ionic liquid C_4C_1ImTFSI on a flat silica surface form step-wise layers similar to crystals.[29] These apparently contradictory phenomena have been rationalized by the hypotheses that both the carbon nanotube and the flat silica surface provide ordered structure with strong enough van der Waals interactions to direct the growth of the ionic liquid crystals, while a similar cohesive interaction fails to assist crystalline ordering in the case of the ionic liquid confined in mesoporous silica.[30,31] Moreover, recent molecular dynamics (MD) simulations of the ionic liquid C_4C_1ImTFSI confined in silica or mesoporous carbon indicate that there is a significant difference in the interaction potential profile close to the silica surface compared to the carbon surface.[25,32]

To understand these phenomena in more detail, the nature and extent of molecular-level ion–ion and ion–wall interactions must be established. As previous studies of ionogels have demonstrated, the combination of 1-alkyl-3-methylimidazolium cations,[8,33,34] and bis(trifluoromethanesulfonyl)imide (TFSI$^-$) anions results in low-melting ionic liquids with high ionic conductivity.[35,36] Therefore, an intermediate chain length ionic liquid, 1-hexyl-3-methylimidazolium bis(trifluoromethanesulfonyl)imide, C_6C_1ImTFSI, was chosen for this study, which displays a high degree of local order yet a reasonably low viscosity.[37,38] In this work, a combination of advanced characterization techniques elucidate the local structure and dynamics of confined C_6C_1ImTFSI ionic liquids, over a wider range of ionic liquid-to-silica molar ratios ($0 \leq x \leq 5$) than has been previously reported. ^{1}H and ^{19}F pulsed field gradient NMR experiments elucidate the concentration dependence of the ionic species' self-diffusivity in the ionogel. Additionally, Raman spectroscopy is used to determine the conformational changes of the ionic species and strength of ion–ion interactions upon confinement. Together, these analyses reveal a molar ratio threshold ($x < 1$) for diffusion, below which the intrinsic ionicity of the ionic liquid is lost. Finally, solid-state two-dimensional (2D) NMR establishes the interactions of the ionic liquid species at the silica surfaces. The molecular-level insights provided by this combination of advanced spectroscopic techniques are expected to be helpful for the design of next-generation ionic liquid-based electrolytes.

2 Experimental

2.1 Ionogel synthesis

Ionogels were prepared following the same sol–gel route described in more detail elsewhere.[34] Typically, samples were prepared directly inside a glass NMR tube, but for those samples with lower volume fraction of ionic liquid that were more brittle, silicon rubber tubes were used to allow the growth of thin crack free monoliths (see Fig. 1). The C_6C_1ImTFSI ionic liquid was purchased from Iolitec and kept in an Ar-gas filled glovebox prior to use. The reactants, tetramethyl orthosilicate (TMOS, 99% purity, Sigma-Aldrich) and formic acid (FA,

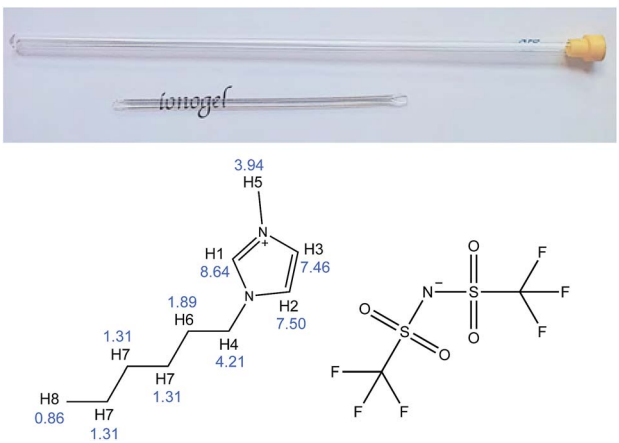

Fig. 1 On the top, a free-standing ionogel ($x = 0.2$) is shown below the NMR tube. In the lower part of the figure the schematic of the ionic liquid 1-hexyl-3-methyl imidazolium bis(trifluoromethanesulfonyl) imide, referred to as C_6C_1ImTFSI in the article, is shown. Proton labeling and ppm shift for respective peak is shown as a guide to the interpretation of the NMR spectra.

¶ Interestingly it is reported that ionogels obtained by swelling previously prepared silica aerogels did not result in changed phase behaviors (*e.g.*, disappearance of liquid–solid transition), as opposed to similar ionogels where the ionic liquid was nano-confined *in situ* during the sol–gel synthesis.[27]

commercially available as 96% by weight in water, Sigma-Aldrich), were mixed together with the ionic liquid. A constant FA to TMOS molar ratio of 4 : 1 was used in all syntheses to ensure a complete reaction of the four methoxy groups in $Si(OCH_3)_4$.[39] The molar ratio, x, of $C_6C_1ImTFSI$ to TMOS were varied over the range of $0 \leq x \leq 5$. After mixing, the reaction went to completion under ambient temperature and pressure conditions. The sol–gel reaction involves hydroxylation, esterification, and condensation that give undesired products such as methyl formate, methanol and water. The majority of these products spontaneously evaporate during reaction and aging (*ca.* weeks), as evidenced by Raman and NMR spectroscopic measurements. However, to remove residual traces of these compounds, the aged gels were further heat treated at 130 °C under N_2 flow for 12 hours.

2.2 N_2 adsorption measurements

The BET (Brunauer–Emmett–Teller) surface area of the ionogels were determined by N_2 adsorption at 77 K on a TriStar 3000 from Micromeritics Instrument Corporation. Before conducting the measurements, the ionic liquid in the ionogels was removed by soaking the gels in ethanol at 55 °C for two hours, after which point the supernatant was replaced with fresh ethanol and the gels were soaked for an additional two hours (repeated for a total of four ethanol washes). The same washing procedure was repeated with acetone. Finally, the sample was ultrasonicated in an ethanol–acetone mixture for one hour, centrifuged, and separated from the supernatant. The washed gel was then dried in an oven at 60 °C. The BET measurements were carried out after the samples were degassed under vacuum at 100 °C overnight.

2.3 Raman spectroscopy

Raman spectra were recorded with an InVia Reflex Renishaw spectrometer using the 785 nm laser wavelength, a 1200 l mm^{-1} grating, a Peltier cooled CCD detector, and a X50 LWD Leica objective. The spectrometer was calibrated to the 1st order band at ~520 cm^{-1} of a Si wafer, displaying a scan-to-scan reproducibility of ±0.2 cm^{-1} and a nominal spectral resolution of 1.2 cm^{-1}. Raman spectra were collected at room temperature on ionogels previously heat treated to eliminate any traces of the by-products from the sol–gel synthesis (methanol, methyl formate, water) and then kept in sealed capillaries to avoid further absorption of moisture. Because of the good quality of the spectra, no further data treatment was needed before spectral analysis.

2.4 Solid-state NMR spectroscopy

Solid-state 2D $^{29}Si\{^1H\}$ HETeronuclear CORrelation (HETCOR) NMR experiments were conducted at 11.7 T using a Bruker AVANCE II spectrometer operating at frequencies of 500.24 MHz for ^1H and 99.38 MHz for ^{29}Si. The experiments were performed at room temperature under magic-angle-spinning (MAS) conditions at 12.5 kHz using a 4 mm Bruker H-X double-resonance probehead and zirconia rotors with Kel-F caps. High-power homonuclear ^1H–^1H decoupling was applied during the ^1H evolution period to enhance the resolution in the ^1H dimension, using the eDUMBO-1 pulse sequence[40] with a phase-modulated radio frequency pulse of constant amplitude (100 kHz). The 2D $^{29}Si\{^1H\}$ HETCOR spectra were acquired with a 2.0 ms contact time and SPINAL-64 ^1H heteronuclear decoupling (80 kHz), using a recycle delay of 1 s and 1536 transients signal-averaged for each of the $95t_1$ increments, resulting in an experimental time of 41 h for each spectrum.

2.5 ^1H and ^{19}F pulsed field gradient NMR spectroscopy

In porous materials, the diffusion that is measured may differ from bulk solution values, depending on the dimensions, tortuosity, and interconnectedness of the pores, as well as the fluids interactions with the pore walls. Due to these effects the term 'apparent self-diffusion' may be more appropriate when discussing the ionic liquid's dynamics within ionogels, as opposed to 'self-diffusion' which is used for bulk ionic liquids. For simplicity and fluency in the text however, we will use only the terms 'diffusion' or 'self-diffusion' coefficient throughout the rest of this paper. The diffusion coefficients (D) of cations and anions were measured by ^1H and ^{19}F NMR, respectively. The ^1H and ^{19}F pulsed field gradient (PFG) NMR experiments were conducted at 14.1 T on a Bruker DMX600 spectrometer operating at frequencies of 600 MHz for ^1H and 564 MHz for ^{19}F. The experiments were performed for a set of temperatures [25, 30, 35, and 40 (±0.1)°C], using a Diff30 diffusion probehead. The pulsed field gradient stimulated-echo (PFGSTE) NMR sequence[41] measures diffusion by acquiring NMR signals at varying magnetic field gradient strengths, G. The diffusion coefficient can then be obtained by fitting the attenuated signal, E, with the Stejskal–Tanner equation:[42]

$$E = \exp[-(\gamma G\delta)^2(\Delta - \delta/3)D] \quad (1)$$

where δ is the gradient pulse duration, Δ is the time lapse between the leading edges of the two gradient pulses, and γ is the gyromagnetic ratio of the probed nucleus. The diffusion measurements were repeated three times with the Δ, δ parameters being varied with respect to each other as a means to check against the occurrence of convection. The Δ, δ parameters were varied within the intervals of 100–500 ms and 0.6–2 ms, respectively, where the lower δ values were used for short T_2 relaxation times. The gradient amplitude, G, was increased linearly within the interval of 0.2 to 10 T m^{-1} in 16 steps. Different lower and upper limits of the gradient strength were chosen depending on the measured diffusion coefficient. Based on the signal-to-noise ratio of the spectrum, between 4 and 512 transients were signal averaged at each gradient step.

Uncertainty in the measured diffusion coefficients is expected to be introduced by obstructed diffusion in the ionogels,[43] internal gradients within the heterogeneous ionogels,[44] magnetization exchange between ionic liquid species,[45,46] and short T_2 relaxation times, especially for ionogels with lower ionic liquid content. The extents to which these factors affect the diffusion coefficients have been assessed in separate experiments. For example, the obstructed diffusion was tested by decreasing Δ to values as low as 10 ms, diffusion coefficient

variations due to internal gradients were tested by utilizing the magic pulsed field gradient pulse sequence,[44] the magnitude of magnetization exchange was tested using the Goldman–Shen experiment,[47] and the effect of short T_2 values was tested by comparing diffusion values measured with longer and shorter δ values (2 ms to 0.6 ms). The results of these sensitivity analyses indicate that the overall trends in the measured diffusion coefficient remains the same.

3 Results and discussion

3.1 Concentration dependent ionic mobility

Fig. 1 shows the molecular structure of the ionic liquid C_6C_1ImTFSI, along with corresponding ^{1}H NMR chemical shift assignments for the protons of the $C_6C_1Im^+$ cation (H1–H8). Consistent with previous studies, we observe that the confinement of the ionic liquid within the ionogel broadens the ^{1}H NMR spectrum, as evidenced in Fig. 2 where ionogels with different ionic liquid-to-silica molar ratios (x) are compared. This broadening becomes especially significant for ionic liquid concentrations of $x < 1$, below which some ^{1}H NMR signals become undistinguishable. Le Bideau *et al.* suggested that this broadening is mainly due to a susceptibility gradient at the pore–wall interface, and showed that a significant part of it can be mitigated by using relatively low magic-angle-spinning (MAS) frequencies, as revealed by the recovery of narrow lines in the solid-state ^{1}H MAS NMR spectra of ionogels with $x = 0.5$.[48] Importantly, their results also indicate that the ionic liquid in the ionogel maintains liquid-like dynamical properties, such that the ions' diffusion coefficients can be reliably measured. In this study, diffusion coefficients have been measured for ionic liquid concentrations as low as $x = 0.2$.

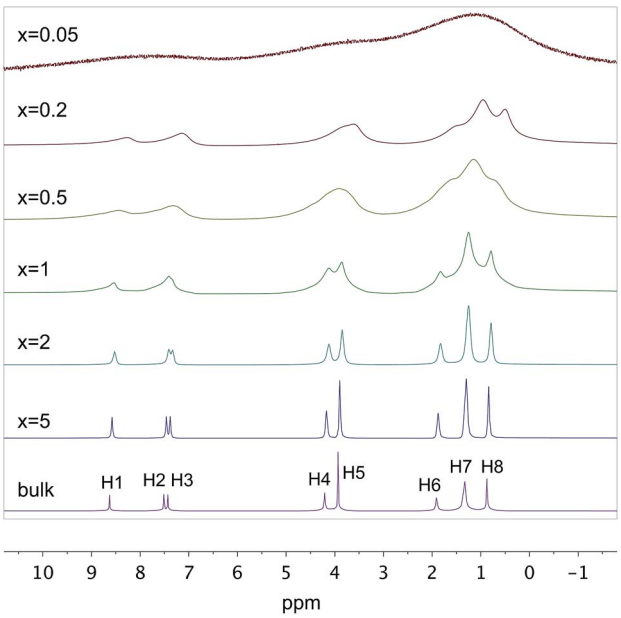

Fig. 2 Solution-state ^{1}H NMR spectra recorded at 313 K for bulk C_6C_1ImTFSI and ionogels with decreasing values of the molar ratio (x) of C_6C_1ImTFSI : SiO_2.

In Fig. 3A, the diffusion coefficients of the cation (D_+) and anion (D_-) measured at 298 K are shown as a function of ionic liquid confinement (*i.e.*, molar ratio of ionic liquid-to-silica precursor). The dashed lines in the upper-left corner correspond to the diffusion coefficients of the $C_6C_1Im^+$ and $TFSI^-$ species in the bulk. It is interesting to note that the imidazolium cation diffuses faster than the anion despite its bulkier structure.[38,49] This anomaly has been attributed to local structural arrangements resulting in a more heterogeneous dynamical environment for the cation with preferential directions of diffusion. In Fig. 3B, the diffusion coefficients in the ionogel are normalized to their bulk values and plotted as a function of the volume fraction of silica, ϕ (top axis).‖ The normalized diffusion coefficients show a clear decrease with increasing silica content, which is qualitatively expected due to the excluded volume effect. To investigate this behavior in more detail, the Maxwell–Fricke model is used to predict values of diffusion for a solvent that is excluded from a volume fraction ϕ:[50–52]

$$D(\phi) = \frac{(1-\phi')D_{\text{bulk}}}{(1+0.5\phi')(1-\phi)}, \quad (2)$$

where D_{bulk} is the bulk diffusion value, $D(\phi)$ is the measured diffusion coefficient as function of the excluded volume fraction and ϕ' accounts for eventual surface-bound solvents that contribute to the overall excluded volume. In the condition that there is no surface-bound solvent, ϕ' becomes equal to ϕ and eqn (2) reduces to:

$$D(\phi) = \frac{D_{\text{bulk}}}{(1+0.5\phi)}, \quad (3)$$

The long-dashed line in Fig. 3B shows how eqn (3) clearly underestimates the decrease in self-diffusivity in the ionogels. Therefore, to model our diffusion data it is needed to account for tightly bound solvation layers, as is the case for many other systems.[53,54] In the Maxwell–Fricke model given in eqn (2) it is presumed that the bound layers are totally immobile. However this might not be true in the case of our system, as recent MD simulation results of ionic liquid diffusion on silica surface would suggest.[32] Therefore, the Maxwell–Fricke model given in eqn (2) is slightly modified to account for the contribution of bound layers to the average measured diffusion coefficient:

$$D(\phi) = \frac{pD_{\text{bulk}}}{(1+0.5\phi')} + (1-p)D_{\text{bound}}, \quad (4)$$

where D_{bound} is the diffusion coefficient of bound ionic liquid and $p = (1-\phi')/(1-\phi)$ is the fraction of ionic liquid not bound to the silica surface. To develop an expression for ϕ' as a function of ϕ, the silica structure in the ionogel is approximated as being composed of small silica particles equal in size and shape, whereby only the concentration of these particles changes with the silica volume fraction. Based on this assumption, the number of ionic liquid layers bound to the silica surface scales proportionally with the silica volume

‖ See ESI-1 for details on estimating volume fraction of ionic liquid and silica from respective molar fraction.

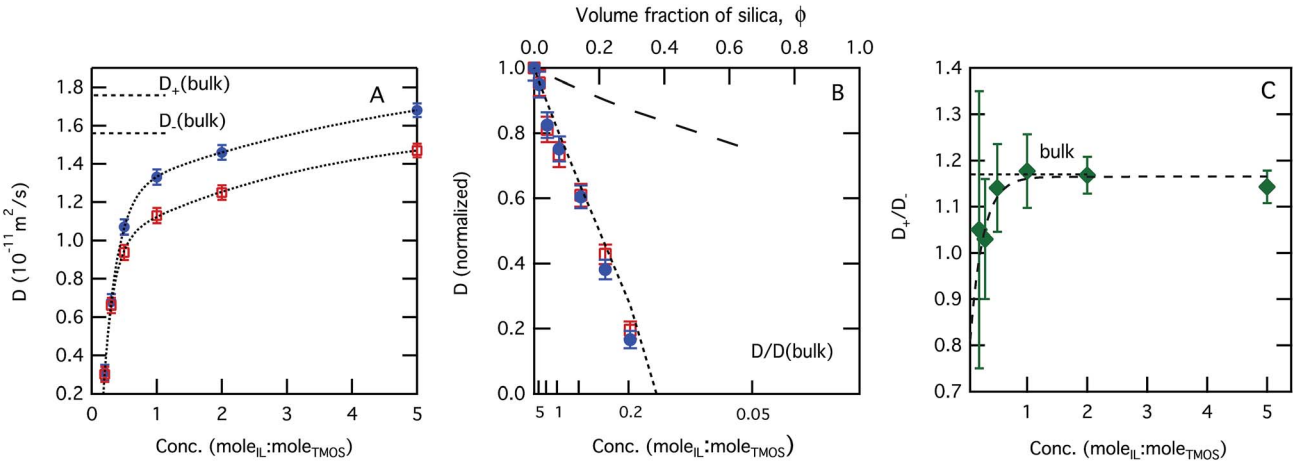

Fig. 3 (A) Diffusion coefficients of the cation (full circle) and the anion (empty square) as a function of ionic liquid concentration, measured at 298 K. The dashed straight lines in (A and C) give the bulk ionic liquid values. The dashed curved lines in (A) are included just as a simple guide to the eye. (B) Same data as (A) but now normalized to the bulk value of the cation and the anion and plotted as a function of a calculated silica volume fraction ϕ given in the upper axis. The long-dashed line and the short-dashed line show the predicted decrease in diffusion given by eqn (3) and (5) respectively. (C) The D_+/D_- ratio as a function of ionic liquid concentration. The error bars given are a combination of repeated experiments and fitting error estimation.

Table 1 BET characterization of ionogels after ionic liquid extraction

X	0	0.05	0.2	0.5	1	2
BET surface area/m^2 g^{-1}	470	750	820	610	710	800

fraction (ϕ), such that doubling the volume fraction doubles the effective silica surface area. Thus, the expression $\phi' = k\phi + \phi$ can be written, where k is a proportionality constant relating the volume of the bound ionic liquid to the volume fraction of silica.** Eqn (4) can then be rewritten as

$$D(\phi) = \frac{(1-(k+1)\phi)D_{\text{bulk}}}{(1-\phi)(1+0.5(k\phi+\phi))} + \frac{k\phi}{1-\phi}D_{\text{bound}}. \quad (5)$$

With the preceding assumptions and with $D_{\text{bound}} \leq 0.04D_{\text{bulk}}$,†† the experimental data can be nicely modeled with $k = 1.5$, as shown by the short-dotted line in Fig. 3B. However, an estimation of the specific surface area available in the silica gels is needed to be able to relate this k value to an approximate number of solvation layers. Based on specific surface areas measured by BET (see Table 1), the k value of 1.5 corresponds to approximately one layer of 'bound' ionic liquid.‡‡ This is in good agreement with recent MD simulation results for a similar system, and further indicates that ionic liquid layers further away from the silica surface exhibit bulk-like dynamics.[32,55]

To better understand the different degrees to which D_+ and D_- are affected by confinement, the D_+/D_- ratio is plotted in Fig. 3C. This plot reveals, especially at very low ionic liquid concentrations, that the diffusion of the cation is more strongly affected by confinement than that of the anion, consistent with the trend observed in Fig. 3A. Similar trends have been reported previously for the ionic liquid C_2C_1ImTFSI, where a stronger interaction between the cation and the silica surface resulted in a greater reduction of the cation's diffusion.[56] Interestingly, a threshold molar ratio of around $x < 1$ is observed in Fig. 3C, below which the intrinsic transport properties of the ionic liquid are more drastically affected by the confinement in silica gels.

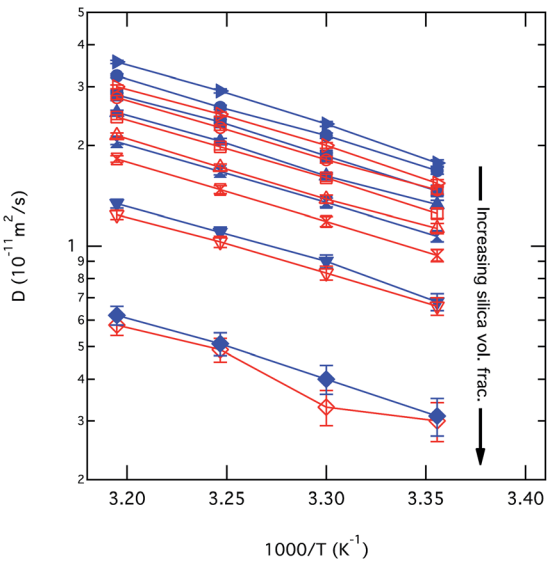

Fig. 4 Diffusion coefficients of the cation D_+ (filled blue symbols) and the anion D_- (empty red symbols) for bulk and confined ionic liquid as a function of temperature in an Arrhenius plot. From top, results are shown for bulk ionic liquid and for x = 5, 2, 1, 0.5, 0.3 and 0.2. The direction of increasing silica volume fraction is also shown.

** For further details on the above calculations see ESI-2.

†† Recent MD simulations for the ionic liquid C_4C_1ImTFSI show that the ionic liquid layer closest to the silica surface would have a reduced diffusion of $D_{\text{bound}} = 0.04D_{\text{bulk}}$.[32]

‡‡ For further details on how these calculations are made see ESI-2.

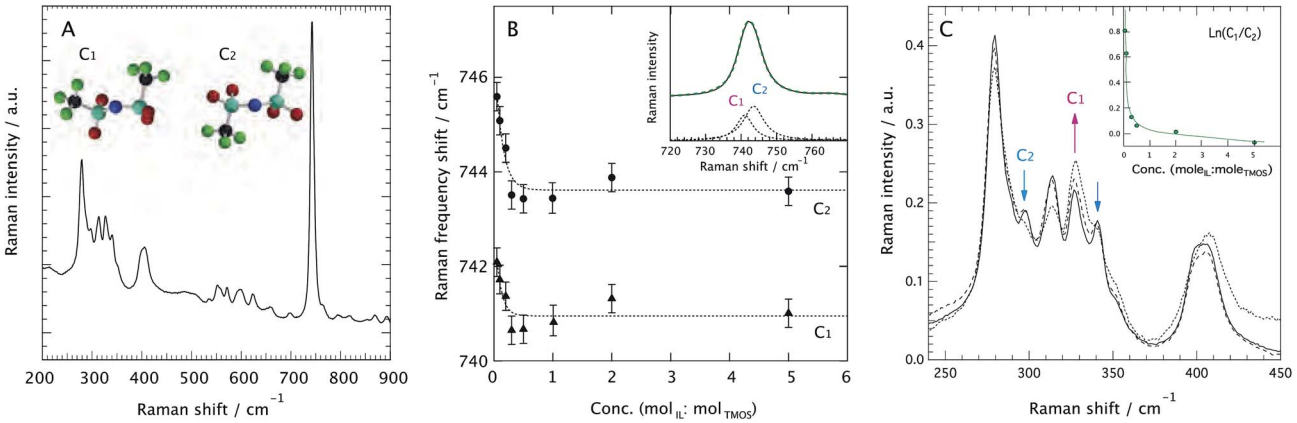

Fig. 5 (A) The Raman spectrum of the ionogel with $x = 0.2$ in the spectral range 200–900 cm^{-1}. Inset: the two conformations of the $TFSI^{-1}$ anion, the *cisoid* (or C_1) and the *transoid* (or C_2). (B) Raman frequency of the two components underlying the main ~740 cm^{-1} Raman signature as a function of ionogel composition. Inset: an example of peak deconvolution using the two-components model, one for each conformational form ($C_1$4 and C_2). (C) Close-up of the conformational sensitive spectral range 200–450 cm^{-1}. Arrows indicate increasing amounts of silica.

The Arrhenius plot in Fig. 4 shows the measured diffusion coefficients of the cation and anion for bulk and confined ionic liquid as a function of temperature. In bulk ionic liquids, the self-diffusion dependence on temperature is very well described by the Vogel–Tamman–Fulcher (VTF) equation:[57]

$$D = D_0 \exp(-B/(T - T_0)). \quad (6)$$

Although the temperature interval investigated here is limited,[§§] wherefore the parameters of the VFT can not be accurately extrapolated, a similar temperature dependence is observed for the confined ionic liquid compared to that in the bulk state. Molecular dynamics simulations reported by Li *et al.*[32] for the ionic liquid C_4C_1ImTFSI confined in silica predict a weaker temperature dependence for ionic liquid layers in direct contact with the pore walls. However, the larger temperature range over which these simulations were performed could explain why a similar effect is not observed in our experiments.

3.2 Local structure and interactions of the ionic liquid species

3.2.1 Conformational state of the ionic liquid. The issue of intermolecular interaction has been addressed by employing Raman spectroscopy. Before collecting Raman spectra, the ionogels were heat-treated to ensure the elimination of reaction products and absorbed moisture. In Fig. 5A, the Raman spectrum of the ionogel with $x = 0.2$ is shown as a representative case. The spectral range 200–900 cm^{-1} contains useful information on both the strength of interaction experienced by the $TFSI^-$ anion (expansion–contraction mode at ~740 cm^{-1}) and its conformational state (240–450 cm^{-1}). Additionally, the inter-tetrahedral Si–O–Si bending mode at ~490 cm^{-1} reveals information about the formation of silica that, by virtue of being a relatively weak Raman scatterer, is evident only for higher silica contents (*i.e.*, for ionogels with $x \leq 0.2$).

The vibrational mode at ~740 cm^{-1} is the most characteristic and strongest Raman signature for $TFSI^-$, and thus has been the focus of previous studies investigating ionic liquids as potential electrolyte materials.[58,59] As a first approximation, the position of this vibrational mode at higher frequencies indicates more strongly bound $TFSI^-$ anions, whereas lower frequencies are representative of more loosely bound anions. By comparison, the LiTFSI salt displays a strong signature at ~747 cm^{-1}.[60] Theoretical calculations have demonstrated that the ~740 cm^{-1} feature is the sum of two components arising from the conformational isomerism of the $TFSI^-$ anion: the *cisoid* (C_1) at ~738 cm^{-1} and the *transoid* (C_2) at ~741 cm^{-1} (inset, Fig. 5B).[60] As previously proposed in other studies,[58,61,62] we employ this model to peak-fit the spectral range 720–760 cm^{-1} (inset, Fig. 5B), and monitor the evolution of the ~740 cm^{-1} feature as a function of ionogel composition. Overall, this mode shifts towards higher frequencies with increasing silica content,[¶¶] which is also the case for the individual components C_1 and C_2. The latter is shown in Fig. 5B, where the Raman frequencies of the two components are compared. While no major frequency changes are observed for ionogels with low silica contents ($x \geq 1$), for higher silica contents ($x < 1$) the mean position of both components markedly shifts towards higher frequencies, as for more bound TFSI anions.

Although the spectral features over the range 720–760 cm^{-1} seem to indicate that the relative population of C_1 and C_2 conformers vary with the ionogel composition, the conformational state of the $TFSI^-$ is in fact better analyzed in the low-frequency range 240–380 cm^{-1}, where vibrational modes are not interaction sensitive.[58] As shown in Fig. 5C, the intensity of the modes associated with the *cisoid* form increase with respect to those of the *transoid* (see arrows) for the ionogels with less ionic liquid (more silica and higher degree of confinement). These

§§ Due to instrumental limitations in the setup used.

¶¶ See first figure in ESI-3.

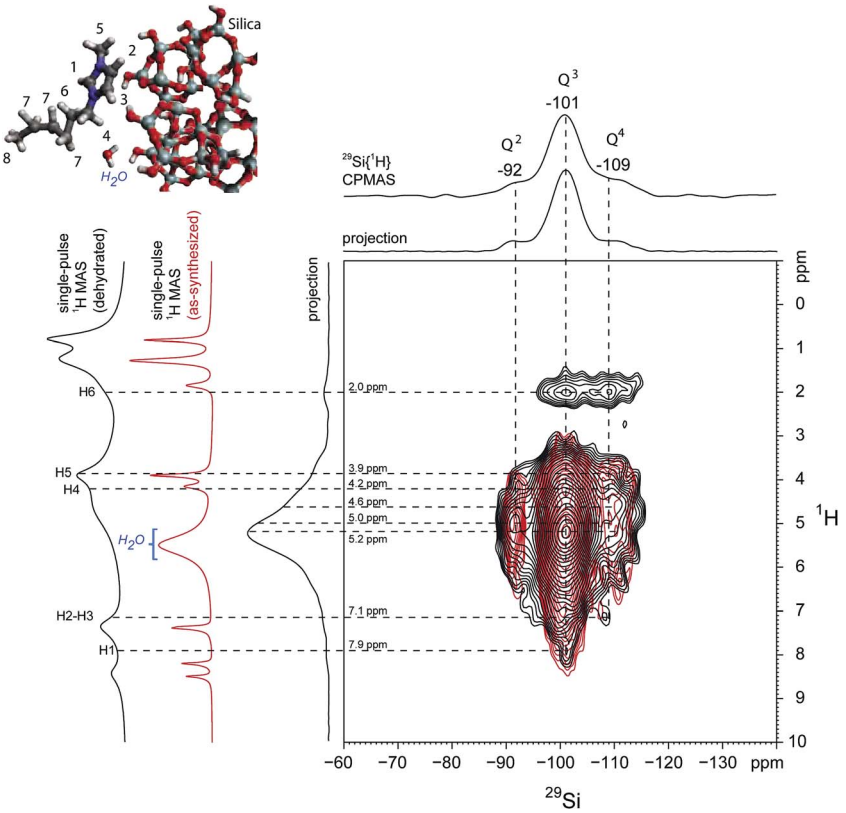

Fig. 6 Solid-state 2D ^{29}Si{^{1}H} HETCOR NMR spectra for the ionogel with the lowest ionic liquid content (C_6C_1ImTFSI : $SiO_2 = 0.05$) before (red) and after (black) dehydration at 130 °C under N_2 flow for 12 hours. A schematic of the relative orientation of the imidazolium cation with respect to the silica surface is shown in the upper left corner of the figure.

results indicate that upon physical constraint, the $TFSI^-$ anions rearrange and establish a conformational equilibrium different from that in the bulk,‖‖ consistent with recently reported results.[34] To quantify these changes, a peak-fit analysis was performed over the spectral range 240–380 cm^{-1} according to the procedure discussed in ref. 58.*** This analysis evidences the increase of the *cis*/*trans* ratio with silica content, as also shown in the inset of Fig. 5C. Interestingly, higher temperatures have also been shown to increase the population of *cisoid* conformers in both protic and aprotic imidazolium ionic liquids.[58,63]

The $C_6C_1Im^+$ cation can also be found in three different conformations that differ in the orientation of the hexyl chain around the C_5–C_6 axis of rotation (see also Fig. 5 in ref. 64). The energies of these conformations are within 4 kJ mol^{-1} of each other, and their respective vibrational signatures indicate that they all coexist in the liquid state. A detailed analysis of the spectral region 450–700 cm^{-1}, where some of these distinct conformational signatures can be distinguished, is shown in ESI-3. A comparison between the Raman spectrum of the pure C_6C_1ImTFSI and that of the ionogel with $x = 0.05$ indicates only a marginal change in the relative intensity of the vibrational mode at 620 cm^{-1}, attributed to the conformational form with a stretched hexyl chain.[64] No further significant changes are observed in the spectrum, suggesting that the three conformers of the imidazolium cation in the ionogels are in the same equilibrium as in the bulk ionic liquid.

3.2.2 Molecular surface interactions of ionic liquid species. Additional insights on the interactions of the ionic liquid species at the silica surface are provided by solid-state 2D NMR methods that are sensitive to dipole–dipole couplings between molecularly proximate (<1 nm) nuclei. For example, the 2D ^{29}Si{^{1}H} HETCOR NMR spectra in Fig. 6 of the ionogel with the lowest C_6C_1ImTFSI ionic liquid content ($x = 0.05$) reveal strong and distinct correlations between ^{29}Si and ^{1}H signals associated with the silica nanoparticles, $C_6C_1Im^+$ species, and water. Two 2D NMR spectra of the ionogel before (red contours) and after (black contours) dehydration, conducted under otherwise identical conditions, are shown for comparison. 1D ^{29}Si{^{1}H} CPMAS and 1D single-pulse ^{1}H NMR spectra are shown along the horizontal and vertical axes, respectively. In addition, 1D projections of the correlated 2D intensities are shown for the dehydrated ionogel sample. The relatively high intensity of the ^{29}Si signal at −101 ppm from Q^3 ^{29}Si species is consistent with the high BET surface area of the silica nanoparticles as measured by N_2 adsorption experiments (see Table 1). By comparison, the signal at −109 ppm is assigned to fully-

‖‖ In bulk ionic liquids an equilibrium of *cisoid* and *transoid* forms is normally found. Below the melting point, however, the *transoid* is the most probable form since it is the conformation of lowest energy.

*** See also ESI-3 for more analysis details.

condensed Q^4 ^{29}Si moieties, while the signal at −92 ppm is attributed to less-condensed Q^2 ^{29}Si sites. Strong 2D correlated signal intensities, which arise principally from dipolar interactions between water molecules and the silica surface, are observed at −92, −101, and −109 ppm in the ^{29}Si dimension and at 5.0, 5.2, and 4.6 ppm in the ^{1}H dimension, respectively. These small variations in ^{1}H chemical shifts are caused by slight differences in local electronic environments of water molecules near ^{29}Si surface species with different extents of hydration. Additional intensity correlations in Fig. 6 are observed for the ^{29}Si signals at −92, −101, and −109 ppm with the various alkyl ^{1}H signals at 2.0 (H6), 3.9 (H5) and 4.2 (H4) ppm, as well as the imidazole proton signals at 7.1 (H2–H3) and 7.9 ppm (H1). Together, these correlated signals establish that the cationic $C_6C_1Im^+$ molecules are molecularly close to the anionic silica surface, as expected due to charge-balancing, electrostatic interactions. Interestingly, the 2D signal intensities between the methylene proton signal at 2.0 ppm (H6) and the ^{29}Si signals at −101 and −109 ppm for the dehydrated ionogel sample (black contours) are not observed under conditions where more adsorbed water is present (red contours). These results indicate that the presence of adsorbed water results in weaker interactions between the silica surface and the hydrophobic alkyl protons of the $C_6C_1Im^+$ molecules. Importantly, these analyses demonstrate how the molecular interactions and dynamics of the ionogel system are strongly influenced by the presence of water, which affects both the hydrophilicity of the silica surface and the mobility of the ionic liquid species.

In separate solid-state 1D single-pulse ^{19}F NMR experiments conducted at room temperature on the dehydrated ionogel sample,††† a narrow ^{19}F signal (3 ppm fwhm) is observed at −80 ppm, corresponding to $-CF_3$ species of the $TFSI^-$. As the temperature is decreased to −40 °C, the ^{19}F signal broadens (5 ppm fwhm), indicating a decrease in mobility of the CF_3 moieties. To establish the extent of interaction of the $TFSI^-$ anions with the silica surface, a solid-state 1D ^{29}Si{^{19}F} CPMAS NMR experiment was performed at −40 °C under 6 kHz MAS, while decoupling ^{19}F. However, no ^{29}Si signal was detected after approximately 3 hours of measurement time, which reflects weak ^{29}Si–^{19}F dipolar couplings and indicates that the $TSFI^-$ anions are more distant from the silica surface than the strongly interacting $C_6C_1Im^+$ cations. This is consistent with the different electrostatic interactions between these ions and the anionic silica surface. Such interactions may partially explain the observed conformational change of the $TFSI^-$ anions (towards more *cisoid* instead of *transoid*) upon higher degrees of confinement, as shown by the Raman analysis of the ionogels (*vide supra*). This finding, together with our results on the local orientation of the $C_6C_1Im^+$ cation, are in overall good agreement with the results obtained by G. Ori *et al.*, who have performed MD simulations on the similar $C_4C_1Im^+TFSI^-$ ionic liquid upon confinement in nano-pores of amorphous and rough silica.[65]

Collectively, these findings establish the molecular interactions of ionic liquids at the silica surfaces, which have been challenging to elucidate. In particular, our experimental results are in agreement with theoretical calculations of the interactions between the ionic liquid $C_4C_1ImPF_6$ and nanoporous silica, suggesting that the imidazolium ring, rather than the alkyl tail, preferentially interacts with the SiO_2 surface moieties.[66] Recently, Nordström *et al.* reported on the solvation shell around Aerosil 200 particles by $LiBF_4$-doped $C_4C_1ImBF_4$, proposing that the BF_4 anions are closer to the silica surface than the C_4C_1Im cations; a different but plausible scenario considering that in this model the Li^+ ions mediate the SiOH$\cdots$ BF_4 interaction.[6] By comparison, in our ionogel systems, the imidazolium species are the only cations present. To the best of our knowledge, no other experimental studies have established the molecular interactions of the ionic liquid species with the silica surface.

4 Conclusions

In the present study, we have investigated the change in dynamical and structural properties of the $C_6C_1ImTFSI$ ionic liquid in nanoporous silica, a type of ionogel, over a wide range of ionic liquid-to-silica concentrations. We make use of a powerful set of advanced spectroscopic methods to elucidate the local transport properties as well as the local structure at the solid–liquid interface.

^{1}H and ^{19}F PFG NMR measurements reveal that the local dynamics of the ionic liquid are strongly dependent on the silica content, and suggest that the translational dynamics of the ionic liquid layer closest to the silica surface are greatly reduced due to ion–wall interactions. Additionally, these results show that the difference in the diffusion coefficient for the cation and anion is decreased for ionic liquid molar ratios of $x < 1$. This observed concentration threshold for ionic mobility is corroborated by stronger ion–ion interactions as evidenced by Raman spectroscopy, based on the Raman frequency shift of the ~740 cm^{-1} vibrational mode characteristic of the $TFSI^-$ anion. Furthermore, although the cation does not undergo significant conformational change in the confined state, the anion shows a clear increase of the *cisoid* forms relative the *transoid* forms in the ionogels.

Solid-state 2D ^{29}Si{^{1}H} HETCOR NMR spectra establish that the $C_6C_1Im^+$ cations strongly interact with the anionic silica surface, where the presence of adsorbed water manifests weaker interactions between ^{29}Si moieties and the hydrophobic alkyl protons of the $C_6C_1Im^+$ cations. In addition, solid-state 1D ^{29}Si{^{19}F} CPMAS NMR measurements indicate that the $TFSI^-$ anions are located further away from the silica surface, compared to the cationic $C_6C_1Im^+$ species. These molecular-level insights about the specific interactions of the ionic liquid moieties at the silica surface are expected to aid in the design of new ionic liquid-derived materials, such as ionogels, for next-generation electrochemical devices.

Acknowledgements

Financial support from the *Energy & Materials* Science Areas of Advance, the Swedish Strategic Research (SSF grant no. ICA10-

††† See figure in ESI-4.

0074), Akzo Nobel, and the National Science Foundation Graduate Research Fellowship under Grant no. 1144085 are all kindly acknowledged. This research is also financially supported by the Institute for Collaborative Biotechnologies through grant W911NF-09-0001 from the U.S. Army Research Office. The content of the information does not necessarily reflect the position or the policy of the U.S. Government, and no official endorsement should be inferred. The solution-state and pulsed field gradient NMR measurements were performed at the Swedish NMR Centre, while the solid-state NMR experiments were conducted at the UCSB MRL Shared Experimental Facilities, the later of which is supported by the MRSEC Program of the NSF under Award no. DMR 1121053. Dr L. Nordstierna, Dr R. J. Messinger, and A. Idström are also acknowledged for fruitful scientific discussions.

References

1 Z. Ma, J. Yu and S. Dai, *Adv. Mater.*, 2010, **22**, 261–285.
2 J. Le Bideau, L. Viau and A. Vioux, *Chem. Soc. Rev.*, 2011, **40**, 907–925.
3 S. Shimano, H. Zhou and I. Honma, *Chem. Mater.*, 2007, **19**, 5216–5221.
4 K. Ueno, Y. Sano, A. Inaba, M. Kondoh and M. Watanabe, *J. Phys. Chem. B*, 2010, **114**, 13095–13103.
5 K. Ueno and M. Watanabe, *Langmuir*, 2011, **27**, 9105–9115.
6 J. Nordström, L. Aguilera and A. Matic, *Langmuir*, 2012, **28**, 4080–4085.
7 R. Göbel, P. Hesemann, J. Weber, E. Möller, A. Friedrich, S. Beuermann and A. Taubert, *Phys. Chem. Chem. Phys.*, 2009, **11**, 3653–3662.
8 M.-a. Néouze, J. L. Bideau, P. Gaveau, S. Bellayer and A. Vioux, *Chem. Mater.*, 2006, **18**, 3931–3936.
9 J.-D. Kim, T. Mori, T. Kudo and I. Honma, *Solid State Ionics*, 2008, **179**, 1178–1181.
10 S. Dai, Y. H. Ju, H. J. Gao, J. S. Lin, S. J. Pennycook, C. E. Barnes, R. Bloomington and A. December, *Chem. commun.*, 2000, 243–244.
11 Y. Shi, Y. Wan and D. Zhao, *Chem. Soc. Rev.*, 2011, **40**, 3854–3878.
12 Y. Zhou, J. H. Schattka and M. Antonietti, *Nano Lett.*, 2004, **4**, 477–481.
13 C.-M. Wu, S.-Y. Lin and H.-L. Chen, *Microporous Mesoporous Mater.*, 2012, **156**, 189–195.
14 M.-A. Néouze, J. Le Bideau and A. Vioux, *Prog. Solid State Chem.*, 2005, **33**, 217–222.
15 Z. Li, H. Liu, Y. Liu, P. He and J. Li, *J. Phys. Chem. B*, 2004, **108**, 17512–17518.
16 M.-A. Néouze, J. Le Bideau, F. Leroux and A. Vioux, *Chem. commun.*, 2005, 1082–1084.
17 P. Wang, S. M. Zakeeruddin, P. Comte, I. Exnar and M. Grätzel, *J. Am. Chem. Soc.*, 2003, **125**, 1166–1167.
18 S. Seki, Y. Kobayashi, H. Miyashiro, Y. Ohno, A. Usami, Y. Mita, N. Kihira, M. Watanabe and N. Terada, *J. Phys. Chem. B*, 2006, **110**, 10228–10230.
19 D. Petit, J.-P. Korb, P. Levitz, J. LeBideau and D. Brevet, *C. R. Chim.*, 2010, **13**, 409–411.
20 A. Noda, M. A. B. H. Susan, K. Kudo, S. Mitsushima, K. Hayamizu and M. Watanabe, *J. Phys. Chem. B*, 2003, **107**, 4024–4033.
21 E. Delahaye, R. Göbel, R. Löbbicke, R. Guillot, C. Sieber and A. Taubert, *J. Mater. Chem.*, 2012, **22**, 17140.
22 J. N. a. Canongia Lopes and A. a. H. Pádua, *J. Phys. Chem. B*, 2006, **110**, 3330–3335.
23 A. E. Bradley, C. Hardacre, J. D. Holbrey, S. Johnston, S. E. J. McMath and M. Nieuwenhuyzen, *Chem. Mater.*, 2002, **14**, 629–635.
24 A. Triolo, O. Russina, H.-J. Bleif and E. Di Cola, *journal of physical chemistry B*, 2007, **111**, 4641–4644.
25 K. S. Han, X. Wang, S. Dai and E. W. Hagaman, *J. Phys. Chem. C*, 2013, **117**, 15754–15762.
26 Y. Lu, S. S. Moganty, J. L. Schaefer and L. a. Archer, *J. Mater. Chem.*, 2012, **22**, 4066–4072.
27 J. Zhang, Q. Zhang, X. Li, S. Liu, Y. Ma, F. Shi and Y. Deng, *Phys. Chem. Chem. Phys.*, 2010, **12**, 1971–1981.
28 S. Chen, G. Wu, M. Sha and S. Huang, *J. Am. Chem. Soc.*, 2007, **129**, 2416–2417.
29 S. Bovio, A. Podestà, P. Milani, P. Ballone and M. G. Del Pópolo, *J. Phys.: Condens. Matter*, 2009, **21**, 424118.
30 M. P. Singh, R. K. Singh and S. Chandra, *journal of physical chemistry B*, 2011, **115**, 7505–7514.
31 K. Nanda, S. Sahu and S. Behera, *Phys. Rev. A*, 2002, **66**, 013208.
32 S. Li, K. S. Han, G. Feng, E. W. Hagaman, L. Vlcek and P. T. Cummings, *Langmuir*, 2013, **29**, 9744–9749.
33 M. A. B. H. Susan, T. Kaneko, A. Noda and M. Watanabe, *J. Am. Chem. Soc.*, 2005, **127**, 4976–4983.
34 A. Martinelli and L. Nordstierna, *Phys. Chem. Chem. Phys.*, 2012, **14**, 13216–13223.
35 H. L. Ngo, K. LeCompte, L. Hargens and A. B. McEwen, *Thermochim. Acta*, 2000, **357–358**, 97–102.
36 B. D. Fitchett, T. N. Knepp and J. C. Conboy, *J. Electrochem. Soc.*, 2004, **151**, E219.
37 J. a. Widegren and J. W. Magee, *J. Chem. Eng. Data*, 2007, **52**, 2331–2338.
38 A. Martinelli, M. Maréchal, A. Ostlund and J. Cambedouzou, *Phys. Chem. Chem. Phys.*, 2013, **15**, 5510–5517.
39 K. G. Sharp, *J. Sol–Gel Sci. Technol.*, 1994, **2**, 35–41.
40 B. Elena, G. de Paëpe and L. Emsley, *Chem. Phys. Lett.*, 2004, **398**, 532–538.
41 W. S. Price, *ChemInform*, 1997, **28**, 299–336.
42 E. O. Stejskal and J. E. Tanner, *J. Chem. Phys.*, 1965, **42**, 288.
43 L. J. Zielinski and P. N. Sen, *J. Magn. Reson.*, 2003, **165**, 153–161.
44 P. Galvosas, F. Stallmach and J. Kärger, *J. Magn. Reson.*, 2004, **166**, 164–173.
45 D. Topgaard and O. Söderman, *J. Phys. Chem. B*, 2002, **106**, 11887–11892.
46 G. Pagès, S. V. Dvinskikh and I. Furó, *J. Magn. Reson.*, 2013, **234**, 35–43.
47 M. Goldman and L. Shen, *Phys. Rev.*, 1966, **144**, 321–331.
48 J. Le Bideau, P. Gaveau, S. Bellayer, M.-a. Néouze and A. Vioux, *Phys. Chem. Chem. Phys.*, 2007, **9**, 5419–5422.
49 A. Noda, K. Hayamizu and M. Watanabe, *J. Phys. Chem. B*, 2001, **105**, 4603–4610.

50 H. Fricke, *Phys. Rev.*, 1924, **24**, 575–587.
51 A. H. Muhr and J. M. Blanshard, *Polymer*, 1982, **23**, 1012–1026.
52 L. Masaro and X. Zhu, *Prog. Polym. Sci.*, 1999, **24**, 731–775.
53 F. P. Duval, P. Porion and H. Van Damme, *J. Phys. Chem. B*, 1999, **103**, 5730–5735.
54 C. Abrahamsson, L. Nordstierna, J. Bergenholtz, A. Altskär and M. Nydén, *Soft Matter*, 2014, 1–3.
55 B. Coasne, L. Viau and A. Vioux, *J. Phys. Chem. Lett.*, 2011, **2**, 1150–1154.
56 K. Ueno, K. Hata, T. Katakabe, M. Kondoh and M. Watanabe, *J. Phys. Chem. B*, 2008, **112**, 9013–9019.
57 H. Tokuda, K. Hayamizu, K. Ishii, M. A. B. H. Susan and M. Watanabe, *J. Phys. Chem. B*, 2004, **108**, 16593–16600.
58 A. Martinelli, A. Matic, P. Johansson, P. Jacobsson, L. Börjesson, A. Fernicola, S. Panero, B. Scrosati and H. Ohno, *J. Raman Spectrosc.*, 2011, **42**, 522–528.
59 J. Pitawala, J.-K. Kim, P. Jacobsson, V. Koch, F. Croce and A. Matic, *Faraday Discuss.*, 2012, **154**, 71–80.
60 M. Herstedt, M. Smirnov, P. Johansson, M. Chami, J. Grondin, L. Servant and J. C. Lassègues, *J. Raman Spectrosc.*, 2005, **36**, 762–770.
61 J. C. Lassègues, J. Grondin, R. Holomb and P. Johansson, *J. Raman Spectrosc.*, 2007, **38**, 551–558.
62 K. Fujii, T. Fujimori, T. Takamuku, R. Kanzaki, Y. Umebayashi and S.-I. Ishiguro, *J. Phys. Chem. B*, 2006, **110**, 8179–8183.
63 A. M. Moschovi, S. Ntais, V. Dracopoulos and V. Nikolakis, *Vib. Spectrosc.*, 2012, **63**, 350–359.
64 J. Kiefer and C. C. Pye, *J. Phys. Chem. A*, 2010, **114**, 6713–6720.
65 G. Ori, F. Villemot, L. Viau, a. Vioux and B. Coasne, *Mol. Phys.*, 2014, **112**, 1350–1361.
66 M. P. Singh, R. K. Singh and S. Chandra, *ChemPhysChem*, 2010, **11**, 2036–2043.